J|A|C|S ARTICLES

Published on Web 10/19/2010

Synthesis and Shape Control of $CuInS_2$ Nanoparticles

Marta Kruszynska, Holger Borchert, Jürgen Parisi, and Joanna Kolny-Olesiak*

University of Oldenburg, Department of Physics, Energy and Semiconductor Research Laboratory, Carl-von-Ossietzky-Str. 9-11, 26129 Oldenburg, Germany

Received May 5, 2010; E-mail: joanna.kolny@uni-oldenburg.de

Abstract: $Cu_2S-CuInS_2$ hybrid nanostructures as well as pure $CuInS_2$ (CIS) nanocrystals were synthesized by methods of colloidal chemistry. The structure, the shape and the composition of these nanomaterials were investigated with transmission electron microscopy (TEM), powder X-ray diffraction (XRD) and energy dispersive X-ray analysis (EDX). By changing the reaction conditions, $CuInS_2$ nanorods with different aspect ratio, dimeric nanorods as well as hexagonal discs and P-shaped particles could be synthesized. Under our reaction conditions, CIS nanoparticles crystallize in the hexagonal wurtzite structure, as confirmed by Rietveld analysis of the X-ray diffraction patterns. The formation of $Cu_2S-CuInS_2$ hybrid nanostructures turned out to be an essential intermediate step in the growth of CIS nanoparticles, the copper sulphide part of the hybrid material playing an important role in the shape control of the CIS nanocrystals. By a treatment of $Cu_2S-CuInS_2$ with 1,10-phenanthroline, Cu_2S parts of the hybrid nanostructures could be removed, and pure CIS nanoparticles with shapes not accessible with other methods can be obtained. Our synthetic procedure turned out to be suitable to synthesize also other compounds, like $CuInS_2-ZnS$ alloys, and to modify, in this way, the optical properties of the nanocrystals.

1. Introduction

Semiconductor nanoparticles attract scientific attention due to their size and shape dependent properties.[1,2] Because of their tunable absorption and emission in the visible and IR range of the solar spectrum, semiconductor nanocrystals are considered as an interesting absorber material for solar cells,[3−6] they are used in light emitting diodes[7] or as fluorescence marker for biomolecules.[8−10] However, most of the best studied materials until now, like cadmium and lead chalcogenides, have a drawback of containing highly toxic components that severely restricts their possible applications.[11,12] A possible alternative material, being less toxic, but having a tunable absorption in the visible range, is copper indium disulfide (CIS), being a direct bandgap semiconductor with a bandgap of ∼1.5 eV in the bulk material and an exciton radius of 4 nm.[13] It has high radiation stability and an extinction coefficient of $\sim 10^5$ cm^{-1} (at 500 nm),[14] a value about 10× higher than that for CdTe.[15] Therefore, CIS is already widely used in thin film solar cells conventionally prepared by sputtering or evaporation techniques.[16−18]

In contrast, there are only few reports about chemical synthesis of colloidal CIS nanoparticles with a narrow size distribution and successful size or shape control.[19] CIS nanocrystals were synthesized by the reaction of copper and indium salts (chlorides,[20−22] iodides,[23] and carboxylates[13,19,23]) with various sulfur sources (dithiocarbamates,[24] thiourea,[22] n-alkylthiols,[13,23] dithiols,[25] elemental sulfur,[19,26] and carbon disulfide[27]) as well as by thermal

(1) Alivisatos, A. P. *J. Phys. Chem.* **1996**, *100*, 13226.
(2) Murray, C. B.; Kagan, C. R.; Bawendi, M. G. *Annu. Rev. Mater. Sci.* **2000**, *30*, 545.
(3) Huynh, W. U.; Dittmer, J. J.; Alivisatos, A. P. *Science* **2002**, *295*, 2425.
(4) Arici, E.; Meissner, D.; Schäffler, F.; Sariciftci, N. S. *Int. J. Photoenergy* **2003**, *5*, 199.
(5) Gur, I.; Fromer, N. A.; Geier, M. L.; Alivisatos, A. P. *Science* **2005**, *310*, 462.
(6) Kumar, S.; Scholes, G. D. *Microchim. Acta* **2008**, *160*, 315.
(7) Rogach, A. L.; Gaponik, N.; Lupton, J. M.; Bertoni, C.; Gallardo, D. E.; Dunn, S.; Pira, N. L.; Paderi, M.; Repetto, P.; Romanov, S. G.; O'Dwyer, C.; Torres, C. M. S.; Eychmüller, A. *Angew. Chem. Int. Ed.* **2008**, *47*, 6538.
(8) Niemeyer, C. M. *Angew. Chem., Int. Ed.* **2001**, *40*, 4128.
(9) Chan, W. C. W.; Nie, S. *Science* **1998**, *281*, 2016.
(10) Bruchez, M. J.; Moronne, M.; Gin, P.; Weiss, S.; Alivisatos, A. P. *Science* **1998**, *281*, 2013.
(11) In Europe, the use of Cd and Pb is banned in electrical components by the "Directive on the restriction of the use of certain hazardous substances in electrical and electronic equipment 2002 95/EC".
(12) Peng, X. *Nano Res.* **2009**, *2*, 425.
(13) Zhong, H.; Zhou, Y.; Ye, M.; He, Y.; Ye, J.; He, C.; Yang, C.; Li, Y. *Chem. Mater.* **2008**, *20*, 6434.
(14) Krunks, M.; Bijakina, O.; Varema, T.; Mikli, V.; Mellikov, E. *Thin Solid Films* **1999**, *338*, 125.
(15) Mitchell, K.; Fahrenbruch, A. L.; Bube, R. H. *J. Appl. Phys.* **1977**, *48*, 829.
(16) Chopra, K. L.; Paulson, P. D.; Dutta, V. *Prog. Photovolt.: Res. Appl.* **2004**, *12*, 69.
(17) Green, M. A. *J. Mater. Sci. Mater. Electron.* **2007**, *18*, S15.
(18) Powalla, M.; Bonnet, D. *Adv. OptoElectron.* **2007**, *2007*, . article ID 97454.
(19) Xie, R.; Rutherford, M.; Peng, X. *J. Am. Chem. Soc.* **2009**, *131*, 5691.
(20) Qi, Y.; Liu, Q.; Tang, K.; Liang, Z.; Ren, Z.; Liu, X. *J. Phys. Chem. C* **2009**, *113*, 3939.
(21) Courtel, F. M.; Paynter, R. W.; Marsan, B.; Morin, M. *Chem. Mater.* **2009**, *21*, 3752.
(22) Koo, B.; Patel, R. N.; Korgel, B. A. *Chem. Mater.* **2009**, *21*, 1962.
(23) Li, L.; Daou, T. J.; Texier, I.; Kim Chi, T. T.; Liem, N. Q.; Reiss, P. *Chem. Mater.* **2009**, *21*, 2422.
(24) Pan, D.; An, L.; Sun, Z.; Hou, W.; Yang, Y.; Yang, Z.; Lu, Y. *J. Am. Chem. Soc.* **2008**, *130*, 5620.
(25) Norako, M. E.; Franzman, M. A.; Brutchey, R. L. *Chem. Mater.* **2009**, *21*, 4299.
(26) Panthani, M. G.; Akhavan, V.; Goodfellow, B.; Schmidtke, J. P.; Dunn, L.; Dodabalapur, A.; Barbara, P. F.; Korgel, B. A. *J. Am. Chem. Soc.* **2008**, *130*, 16770.

 10.1021/ja103828f

decomposition[28] or irradiation[29] of single molecule precursors. However, these synthetic procedures involving Cu, In, and S do not always result in the formation of monophasic CIS particles, but also hybrid materials, e.g., composed of $Cu_2S-In_2S_3$ can occur.[30,31] There is also one report about CIS nanorods growing on Cu_2S nanodiscs, which can be converted to CIS in the end of the reaction.[32] To summarize, development of synthetic procedures yielding pure CIS nanoparticles with well controllable size and shape still remains a challenge.

Concerning the crystal structure, it is noteworthy that bulk CIS at room temperature has the chalcopyrite crystal structure, whereas the zinc blend and wurtzite modifications are stable only at high temperatures. In contrast, nanoparticles stable at room temperature can be synthesized in all three crystal structures.[33,34] In the zinc blend and wurtzite structure, the indium and copper atoms are randomly distributed over the cation sites of the lattice,[20] which allows a flexibility of stoichiometry and, thus, tuning the Fermi energy over a wide range. The latter feature makes CIS nanoparticles particularly interesting for device fabrication.

Herein, we report a colloidal synthesis of wurtzite CIS nanocrystals as well as Cu_2S-CIS nanohybrids, using simple and commercially available chemicals as starting materials. Even though our synthesis is a one pot reaction, the growth mechanism of CIS nanocrystals involves several steps, their progression being determined by the starting conditions of the reaction. As will be shown, the reaction starts by the formation of copper sulphide nanoparticles, which serve as starting points for the subsequent growth of CIS nanocrystals and play a major role in the shape control of the resulting CIS particles. Cu_2S disappears in the course of the reaction, so that monophasic CIS nanoparticles are the final product. By stopping the reaction at an intermediate stage, $Cu_2S-CuInS_2$ hybrid nanostructures can be obtained. Upon changing the reaction conditions (ratio between the precursors and reaction time), a variety of different shapes of CIS nanoparticles and $Cu_2S-CuInS_2$ nanohybrid materials can be synthesized. In the present work, we describe their formation mechanism and structure, based on TEM, XRD, and EDX measurements.

2. Experimental Section

2.1. Materials. Copper(I) acetate (CuAc, 97%), zinc acetate ($ZnAc_2$ 99.99%, metal basis), technical grade trioctylphosphine oxide (TOPO, 90%), 1-dodecanethiol (1-DDT, 98+%), *tert*-dodecanethiol (*t*-DDT, 98.5%, mixture of isomers) and 1,10-phenanthroline (≥99%) were purchased from Aldrich. Indium(III) acetate ($InAc_3$, 99.99%, metal basis) and trioctylphosphine oxide (TOPO, 98%) were delivered from Alfa Aesar and oleylamine (OLAM, ~C18-content 80−90%) from Acros Organics. All chemicals were used directly without any further purification.

2.2. Synthesis of $CuInS_2$ Nanocrystals. For a typical synthesis, CuAc (1 mmol), $InAc_3$ (1 mmol) and TOPO (90%) (3.5 mmol) were mixed with 10 mL of oleylamine in a three-neck flask and stirred under vacuum at room temperature for 30 min. Next, the reaction was heated to 240 °C under nitrogen flow. When the solution color changed from turbid green to slightly yellow, the mixture of 0.25 mL 1-DDT and 1.75 mL t-DDT was rapidly injected, which resulted in an immediate color change of the reaction solution to brown. Small aliquots were taken at different time intervals between 30 s and 1 h. Finally, the reaction system was cooled to room temperature, and the particles were precipitated and washed with ethanol to remove residual thiols, acetates and TOPO. The purified precipitate was then redissolved in hexane. It is anticipated in this place that CIS nanoparticles prepared by this method can contain an attached Cu_2S particle, depending on the exact reaction conditions and growth time.

2.3. Synthesis of $CuInS_2-ZnS$ Nanocrystals. The first step of the $CuInS_2-ZnS$ nanocrystal synthesis was performed similarly to the reaction for CIS, i.e., indium and copper acetates and TOPO were dissolved in oleylamine and heated to 240 °C. Next, the mixture of thiols and, subsequently, zinc acetate (2 mmol) in 2 mL of OLAM were injected, and aliquots were taken at different times. Afterward, a purification procedure with ethanol was used, as described above for the CIS nanocrystals.

2.4. Transformation of Biphasic $Cu_2S-CuInS_2$ to Monophasic $CuInS_2$ Nanocrystals. In order to eliminate the Cu_2S structural constituent, biphasic nanocrystals were precipitated with methanol, redispersed in a 0.4 M 1,10-phenanthroline solution in ethanol, and stirred at room temperature for 17 or 24 h. The nanoparticles were separated from the characteristically red colored solution, proving the formation of copper-phenanthroline complex, by centrifugation, and subsequently redissolved in hexane.

2.5. Characterization Methods.

2.5.1. UV−vis Absorption Spectroscopy. Absorption spectra were measured on a Varian Cary 100 Scan spectrophotometer.

2.5.2. Transmission Electron Microscopy (TEM). Nanocrystal size and morphology were studied with a Zeiss EM 902A transmission electron microscope with an acceleration voltage of 80 kV. High resolution transmission microscopy observations as well as energy-filtered TEM measurements were performed on a FEI Titan 80/300 kV microscope. Nanocrystals in hexane solution were deposited onto the carbon-coated copper or nickel grids by drop casting technique.

2.5.3. Energy dispersive X-ray Analysis. The integral stoichiometry was obtained by the EDAX detector integrated into a FEI Quanta 200 3D scanning electron microscope. Stoichiometry of individual nanoparticles was analyzed with the EDX detector of the FEI Titan 80/300 kV microscope.

2.5.4. Powder X-Ray Diffraction (XRD). Powder X-ray diffraction (XRD) was measured with a PANalytical X'Pert PRO MPD diffractometer operating with Cu K_α radiation, Bragg−Brentano $\theta-2\theta$ geometry, a goniometer radius of 240 mm and variable slits. The samples were measured on low background silicon sample holders and prepared for the XRD measurements as follows: Nanocrystals in hexane solution were dropped on the silicon substrate and heated to 70 °C for 30 min, in order to remove the solvent.

The XRD data was analyzed using the X'Pert HighScore Plus software in conjunction with the ICDD database, version 2.0902. For Rietveld refinement, the program MAUD,[35] version 2.14, was used. In all cases, a polynomial background was used. The parameters for instrumental line broadening were not refined, but taken from the default instrument in the MAUD software. This is justified, because the line broadening is dominated by size and strain effects in the case of nanocrystalline samples. Texture effects were taken into account by the harmonic texture model[36] implemented into the MAUD program, using the parameter $L_{max} = 4$ which

(27) Du, W.; Qian, X.; Yin, J.; Gong, Q. *Chem.—Eur. J.* **2007**, *13*, 8840.
(28) Castro, S. L.; Bailey, S. G.; Raffaelle, R. P.; Banger, K. K.; Hepp, A. F. *J. Phys. Chem. B* **2004**, *108*, 12429.
(29) Nairn, J. J.; Shapiro, P. J.; Twamley, B.; Pounds, T.; Wandruszka, R. V.; Fletcher, T. R.; Williams, M.; Wang, C.; Norton, M. G. *Nano Lett.* **2006**, *6*, 1218.
(30) Han, W.; Yi, L.; Zhao, N.; Tang, A.; Gao, M.; Tang, Z. *J. Am. Chem. Soc.* **2008**, *130*, 13152.
(31) Choi, S.; Kim, E.; Hyeon, T. *J. Am. Chem. Soc.* **2006**, *128*, 2520.
(32) Connor, S. T.; Hsu, C.; Weil, B. D.; Aloni, S.; Cui, Y. *J. Am. Chem. Soc.* **2009**, *131*, 4962.
(33) Binsma, J. J. M.; Giling, L. J.; Bloem, J *J. Cryst. Growth* **1980**, *50*, 429.
(34) Nose, K.; Soma, Y.; Omata, T.; Otsuka-Yao-Matsuo, S. *Chem. Mater.* **2009**, *21*, 2607.
(35) Lutterotti, L.; Chateigner, D.; Ferrari, S.; Ricote, J. *Thin Solid Films* **2004**, *450*, 34–41.

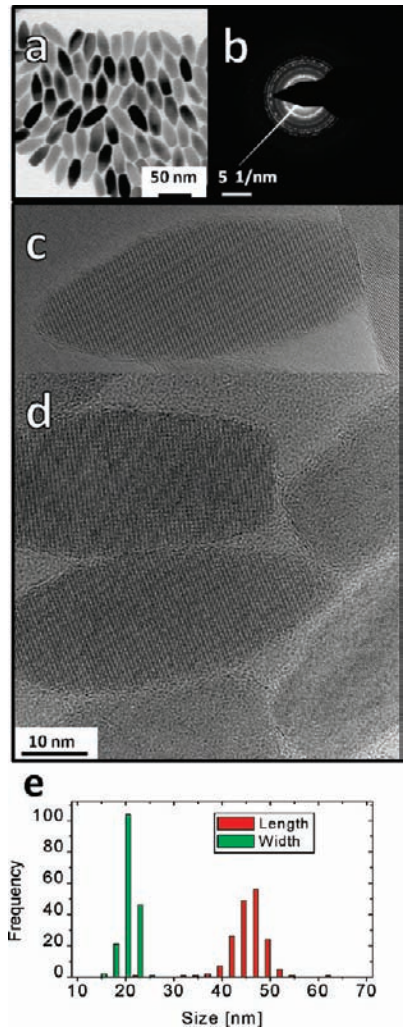

Figure 1. An overview TEM image of a typical CIS sample (a), SAED pattern (b), HRTEM images of single CIS nanoparticles (c) and (d), and a histogram of the width and the length of the nanocrystals (e).

corresponds to 2 variables for refinement. Furthermore, the anisotropic size-strain model developed by Popa[37] was used to take care of the anisotropic crystallite shape, again using $L_{max} = 4$. This corresponds to 3 variables for the anisotropic crystallite shape and 1 free variable for isotropic strain.

3. Results and Discussion

3.1. Colloidal Synthesis of Uniform $CuInS_2$ Nanocrystals. In this section, we present a synthesis route for pure $CuInS_2$ nanocrystals and give a detailed analysis of a typical sample. Copper indium disulfide nanocrystals were obtained by fast injection of a mixture of 1-dodecanethiol and *tert*-dodecanethiol to a solution of copper and indium acetates in oleylamine and TOPO. The reaction was carried out at 240 °C and yielded elongated wurtzite CIS nanoparticles with a relatively narrow size distribution (Figure 1). The choice of oleylamine as solvent turned out to be essential to obtain a narrow size and shape distribution. A control experiment with 1-octadecene as solvent led to the formation of much smaller particles with a relatively broad size distribution and a higher aggregation tendency. So, OLAM not only plays the role of a solvent, but also regulates the activity of the monomers and stabilizes the particles. However, to provide a good colloidal stability of the particles and to obtain anisotropic shapes, TOPO has to be present in the reaction mixture. TOPO and phosponic acids which are present as impurities in commercially available TOPO[38,39] are hard Lewis bases and react preferentially with In^{3+}, a hard Lewis acid. The presence of TOPO in the reaction mixture decreases and regulates the reactivity of the indium precursor.

We chose *tert*-dodecanethiol as a sulfur source, since thiols are known to decompose at high temperatures.[13,23] *Tert*-dodecanethiol has the advantage of being liquid, soluble in organic solvents and to decompose at relatively low temperatures, compared to *n*-alkyl thiols. The presence of 1-dodecanethiol in the reaction mixture turned out to be necessary to control the reactivity of the copper monomers. Thiols are soft bases and react preferentially with soft acids like Cu^+. *Tert*-dodecanethiol reacts with copper acetate to form copper sulphide already at about 60 °C. In the presence of 1-dodecanothiol, this reaction can be suppressed, and the formation of CIS nanoparticles takes place. The synthesis of CIS nanoparticles can be conducted by mixing the educts at room temperature and subsequently heating them to 240 °C. However, in order to improve the size distribution of the samples, we decided to start the reaction at high temperature (240 °C) by the injection of the thiols. In this way, the nucleation of the nanoparticles can be controlled in a precise way.

In Figure 1a, a TEM image of a typical sample obtained with our synthetic procedure is shown. The nanoparticles are uniform in size and shape, having a mean width of 19.1 ± 1.4 nm and a length of 44.8 ± 3.8 nm (Figure 1e). These values obtained from TEM images (assuming an elliptic shape of the nanoparticles for the computer-assisted image analysis) are in good agreement with the values calculated from the powder X-ray diffraction patterns (see below). The width of the nanoparticles is not uniform. They consist of two cones with different angles, one being truncated and their footings meeting at about the half of the particle. This general structure could be found in most of the samples obtained at different synthetic conditions and is a direct consequence of the formation mechanism of the CIS particles, as will be discussed later.

High resolution TEM images reveal that the particles are single crystalline and the spacing of the lattice planes corresponds to the wurtzite CIS structure. In the electron diffraction image distances corresponding to (100), (002), (101), (102), (110), (103), and (112) could be identified (Figure 1b). An analysis of the high resolution TEM (HRTEM) images of single particles shows that the nanocrystals grow in the direction of the *c* axis. In Figure 1c,d, examples of particles with (002) lattice planes being perpendicular to the growth direction of the nanocrystals are shown.

CIS is known to differ often from the exact 1:1:2 stoichiometry. By the help of EDX measurements, we could confirm the composition of our nanoparticles being close to 1:1:2, however, with a small In excess (Cu:In ~4:5). The EDX results show also a small excess of sulfur, the atomic ratio S/(Cu+In) being ~1.1. This could be due to a sulfur rich surface, which is a plausible assumption when using thiols as stabilizer. Even if the particles do not have the perfect 1:1:2 stoichiometry, we will refer to them as $CuInS_2$ for the sake of simplicity. In order to exclude the possibility that our nanorods are nanocomposites of copper and indium sulphide, similar to particles described

(36) Popa, N. C. *J. Appl. Crystallogr.* **1992**, *25*, 611.

(37) Popa, N. C. *J. Appl. Crystallogr.* **1998**, *31*, 176.
(38) Wang, F.; Tang, R.; Buhro, W. E. *Nano Lett.* **2008**, *8*, 3521.

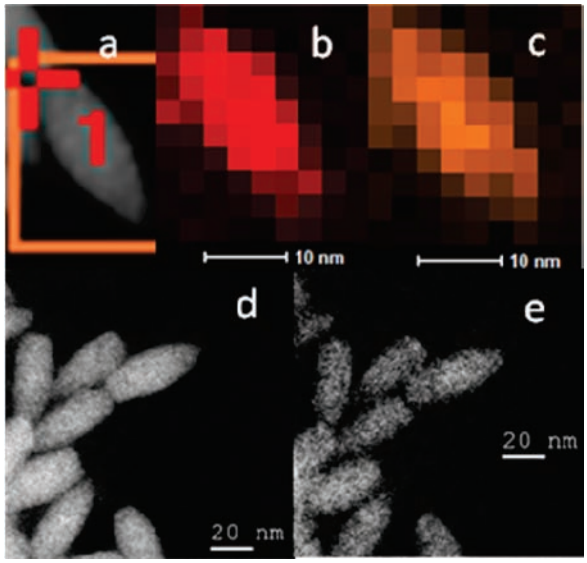

Figure 2. STEM image of a single CIS nanoparticle (a) together with its copper (b) and indium (c) map obtained by spatially resolved EDX measurements. The distribution of sulfur (d) and copper (e) in the sample was measured with energy filtered STEM.

in refs 30 and 31, rather than monophasic CIS nanoparticles, we investigated also the composition of single particles by energy filtered scanning TEM (STEM) and EDX. Figure 2a shows a single particle. In Figure 2b,c, spatially resolved EDX measurements of this particle can be seen, revealing the uniform distribution of copper and indium within the particles. Energy filtered dark field images in Figure 2d,e show that also sulfur and copper are uniformly distributed. So, all three elements can be found throughout the particles.

Figure 3a shows the powder X-ray diffraction pattern measured for the sample analyzed above by TEM. The crystal structure was identified to be hexagonal $CuInS_2$ (see Supporting Information for details on the structure). CIS prepared by methods used in industrial processes, e.g., sputtering techniques, typically has a tetragonal or cubic structure.[16] However, hexagonal structure was already observed for colloidally prepared CIS nanocrystals by several other groups.[20,22,24,32] In most cases, the hexagonal CIS phase was identified by comparing the experimental diffraction to simulated stick patterns, because there is no reference data for hexagonal CIS in the standard databases yet.[22,24,32] While the positions of the Bragg reflections were found to match well, less attention was usually paid to the relative intensities or line broadening. In some cases, the match of intensity patterns is relatively poor. In the present work, Rietveld refinement was used, in order to analyze also the intensity distribution and anisotropic line broadening effects. As will be shown in the following, this allows for obtaining important information on the microstructure of the samples.

As obvious from the TEM images (Figure 1), the nanocrystals have an elongated shape. If the direction of preferential growth corresponds to the axis of highest symmetry, i.e., the *c*-axis in the case of hexagonal structure, then the crystallite shape can be simulated by a model developed by Popa[37] that uses a development into a series of symmetrized spherical harmonics. Additionally, the Popa model describes microstrain, where the coefficient $\langle\varepsilon_{hh}\rangle$ represents the relative changes of the distances between the lattice planes in a crystallographic direction denoted *h*.[37] Closely related to anisotropic crystallite shapes, one has to consider texture effects, because elongated crystallites will not

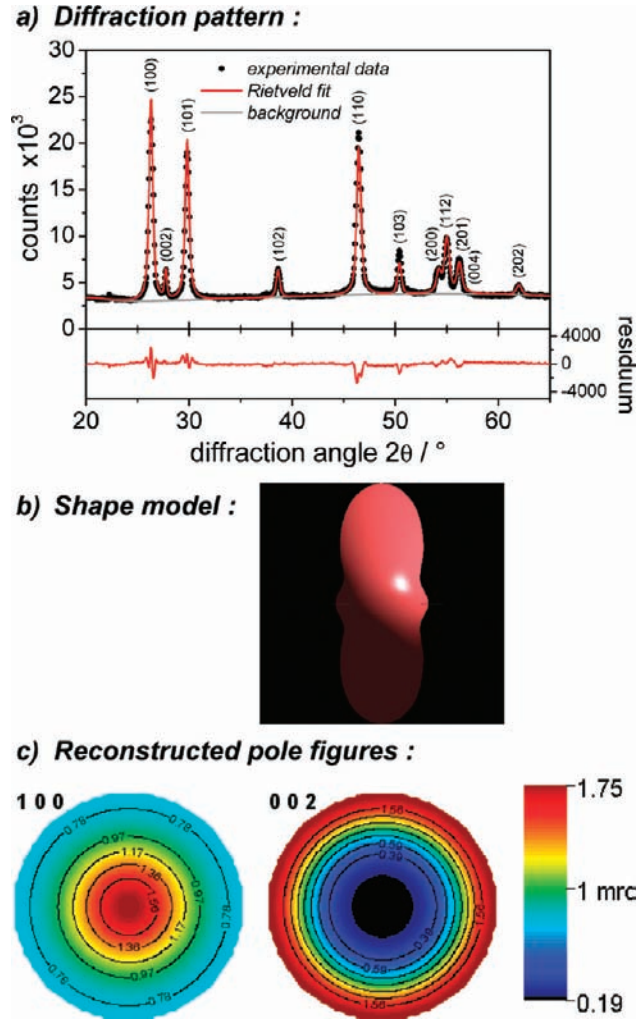

Figure 3. (a) Diffraction pattern of the sample characterized by TEM in Figures 1 and 2. The experimental data (dots) is plotted together with a Rietveld fit (red line). (b) The crystallite shape resulting from refinement according to the applied size-strain model. (c) Reconstructed pole figures resulting from refinement according to the applied texture model. While the (100) planes have a high probability to be oriented parallel to the sample holder, the (002) planes are preferentially oriented perpendicular to the sample holder.

be randomly oriented, but are more likely to lie flat on the sample holder.

If the crystallite shape is assumed to be a sphere and preferential orientation is neglected, then the positions of the Bragg reflections are well matched, but the intensity distribution is not (see Figure S1 of the Supporting Information). The fit in Figure 3a was obtained taking into account the anisotropic microstructure and preferential orientation. Figure 3b shows the simulated crystallite shape resulting from refinement. Table 1 (column "fit 1") sums up the most important parameters and results. The analysis revealed that the nanocrystals are elongated along the *c*-axis, and the values found for the size along the *c*-axis (correlated with the broadening of the (002) reflection) and perpendicular to the *c*-axis (e.g., correlated with the broadening of the (100) reflection) are in good agreement with the TEM results. Figure 3c shows reconstructed pole figures deduced from the simultaneous texture analysis. The poles of the (002) lattice planes are found preferentially in the circumference of the projection plane, meaning that the elongated nanocrystals preferentially lie flat on the sample holder. By

Table 1. Parameters and Results from Rietveld Refinement of the Diffraction Pattern of the Sample Shown in Figures 1−3

	fit 1	fit 2	fit 3	fit 4	fit 5	fit 6
curve in Figure	3a	S2	S1,S3	S3	S3	not shown
shape	anisotropic	anisotropic	isotropic	isotropic	isotropic	anisotropic
size/strain refinement	size refined before strain	simultaneously	simultaneously	simultaneously	simultaneously	size refined before strain
texture	yes	yes	no	no	no	yes
composition	$Cu_1In_1S_2$	$Cu_1In_1S_2$	$Cu_1In_1S_2$	$Cu_{0.5}In_{1.5}S_{2.5}$	$Cu_{1.5}In_{0.5}S_{1.5}$	$Cu_{0.81}In_{1.01}S_2$
occupancy Cu	0.5	0.5	0.5	0.25	0.75	0.404
occupancy In	0.5	0.5	0.5	0.75	0.25	0.505
occupancy S	1.0	1.0	1.0	1.25	0.75	1.0
unit cell par.	3.9062	3.9062	3.9062	3.9062	3.9062	3.9062
a, b [Å]	±0.0002	±0.0002	(fixed)	(fixed)	(fixed)	±0.0002
unit cell par.	6.4251	6.4240	6.4251	6.4251	6.4251	6.4252
c [Å]	±0.0010	±0.0009	(fixed)	(fixed)	(fixed)	±0.0010
atomic pos.	0.3711	0.3699	0.3711	0.3711	0.3711	0.3656
z (Cu,In)	±0.0014	±0.0014	(fixed)	(fixed)	(fixed)	±0.0013
size along *c* axis [nm]	56.3	107.2	21.4	21.3	21.8	54.6
size ⊥ *c*-axis [nm]	21.3	23.09	21.4	21.3	21.8	21.1
strain $<\varepsilon_{hkl}>$, in %	0.16	0.22	0.13	0.14	0.14	0.16
R_P, in %	4.09	4.03	10.4	10.5	10.3	3.94
R_{WP}, in %	5.51	5.35	18.2	18.4	18.1	5.24

consequence, the (100) planes are preferentially oriented parallel to the sample holder which results in a high density of poles in the center of the corresponding pole figure.

It should be noted that parameters for size and strain were not simultaneously varied to obtain the results shown in Figure 3. First, the parameters for anisotropic crystallite size were refined neglecting strain (parameters set to zero). Afterward, size parameters were fixed, and the strain parameters were refined in addition. Refining all size and strain parameters simultaneously slightly improved the fit, but the results were suspicious. Larger values for the strain led to values for the crystallite size in c-direction which considerably exceeded the values found by TEM (see Table 1 (column "fit 2") and Figure S2 of the Supporting Information). The size effects seem to dominate over strain effects, and fitting first the size and, in a second step, the strain parameters appears to be more reliable here. Considering both procedures, one can conclude that the length of the crystallites along the *c*-axis is at least ∼56 nm according to XRD. Together with the TEM data which revealed a mean length of ∼45 nm, this is a good proof that most nanocrystals of the ensemble are elongated along the *c*-axis and consist of one single crystalline domain. Otherwise, the (002) reflection would be broader.

Another remark is necessary with respect to elemental composition. Pan et al.[24] simulated Cu−In−S compounds with various compositions in the case of cubic crystal structure. The diffraction pattern turned out to be unaffected as long as the valence stoichiometry parameter, defined as (2[S]/([Cu]+3[In]))−1, is zero.[24] Similar investigations were made in the present study for the case of hexagonal crystal structure. The intensities turned out to be only slightly dependent on the Cu/In ratio, while keeping the valence stoichiometry parameter at zero (see Figure S3 of the Supporting Information). By consequence, XRD is not suitable to determine the exact composition of the Cu−In−S compounds. According to the EDX results, the valence stoichiometry parameter is close to zero. Therefore, analyzing the XRD data with a stoichiometric $CuInS_2$ phase is reasonable. Using the stoichiometry derived by the values of the EDX ratio and setting the occupancy of S sites to 1 results only in a negligible improvement of the fits (see Table 1 (column "fit 6")).

Turning now to optical properties, all particles synthesized with our method absorb light in the whole visible range (see Figure 4) which results in a black color of the material. The absorption onset reveals a bandgap of 1.5 eV. Because of the small exciton radius in CIS (4 nm), no blue shift due to the size quantization effect can be expected, since our particles have sizes in the order of magnitude of tens of nanometers. Their bandgap can, however, be influenced by doping the particles with Zn, as will be discussed in the last section of the Results and Discussion part.

3.2. Characterization of the Cu_2S−$CuInS_2$ Hybrid Nanocrystals. Cu_2S−$CuInS_2$ hybrid nanocrystals are an important intermediate step in the growth of CIS nanoparticles. The formation of a hybrid material in the beginning of the reaction can be seen in the TEM images, where each particle is composed of two parts of different contrast (see Figure 5a). EDX measurements of these structures show a high copper excess (Cu:In ≈ 4:1), compared to the CIS stoichiometry. A further structural characterization was done by the analysis of the diffraction pattern of the hybrid nanoparticles. Figure 6a shows the diffraction pattern of such a composite sample. By Rietveld analysis, the diffraction pattern can be decomposed into two contributions, one of them being a hexagonal CIS phase as in the former section, the other being a hexagonal Cu_2S phase. The crystal structure of the Cu_2S phase was taken from a

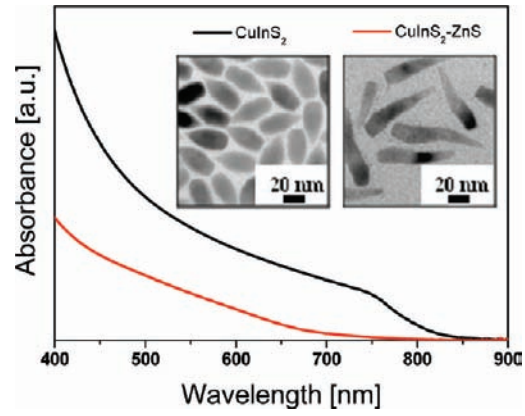

Figure 4. Typical absorption spectra of pure $CuInS_2$ and alloyed $CuInS_2$−ZnS nanocrystals.

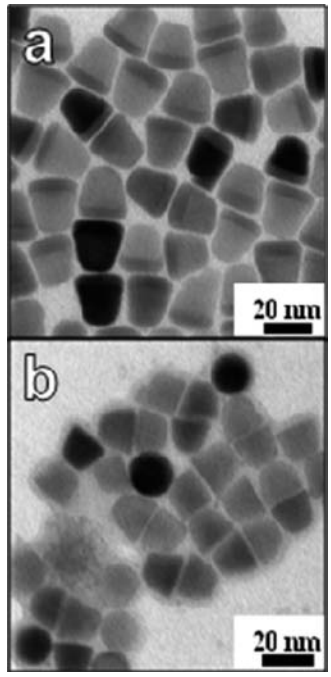

Figure 5. $Cu_2S-CuInS_2$ before (a) and $CuInS_2$ nanoparticles after (b) treatment with 1,10-phenanthroline. The sample in (a) was obtained after a reaction time of 1 min.

database entry based on ref 39, and results for the most important fitting parameters can be found in the Supporting Information (Table S2). Size-shape analysis (see also Figure 6b) revealed a disk-like shape for the Cu_2S part with ~4 nm thickness and ~13 nm diameter which is in reasonable agreement with the TEM image shown as inset in Figure 6a. The short axis corresponds to the *c*-axis of the hexagonal structure. The lattice parameters *a* and *b* being almost identical for both phases, the CIS phase can epitaxially grow on top of the Cu_2S part. Sizes determined by XRD for the CIS part are also in reasonable agreement with the TEM images. Thus, the XRD analysis clearly confirms that these particles are composite structures of two materials, CIS and Cu_2S.

1,10-Phenanthroline reacts selectively with Cu^+ ions, and so it is possible to remove the copper sulphide part of the hybrid particles.[30] A comparison of TEM images of hybrid nanoparticles before and after phenanthroline treatment (see Figure 5) helps to identify the disk shaped part of the hybrid material (disappearing after the reaction with phenanthroline) as copper sulphide, which is in accordance with the results of the analysis of the diffraction pattern of these particles.

Control experiments with pure CIS nanoparticles treated with phenanthroline show no change in the shape and the structure of the material (see Figures S6 and S7 of the Supporting Information). However, also in these experiments dissolution of copper ions can be observed. Phenanthroline forms a red colored complex with copper(I) ions. This red color appears both in reactions with CIS nanoparticles and Cu_2S-CIS hybrid materials. However, in the case of pure CIS, conservation of the particle size and shape suggests that only surface copper atoms are removed by the reaction with phenanthroline. Removal of the copper(I) ions by phenanthroline treatment opens up the possibility to obtain more differently shaped CIS

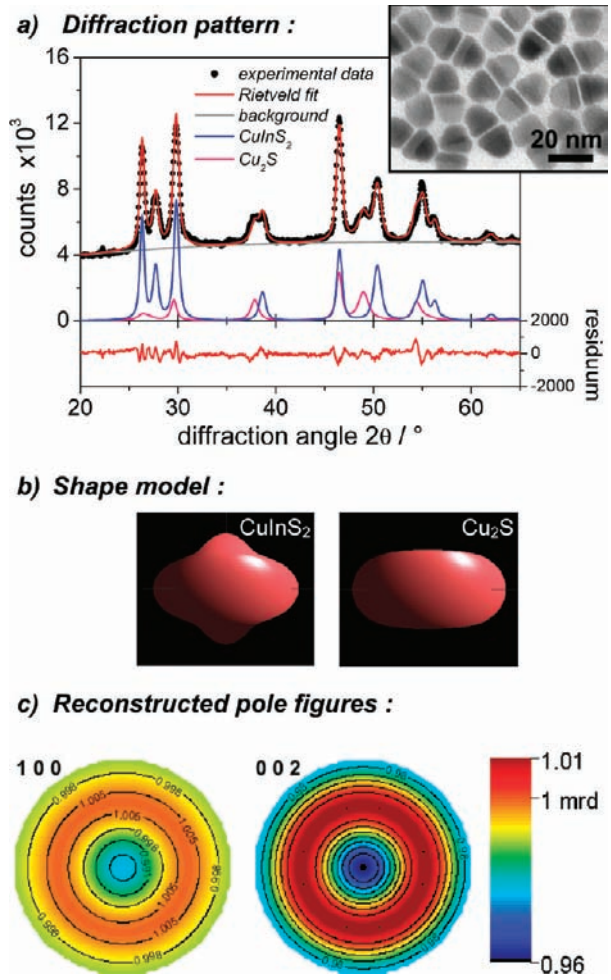

Figure 6. (a) diffraction pattern of a typical $Cu_2S-CuInS_2$ sample (inset: TEM image). The experimental data (dots) is plotted together with a Rietveld fit (red line) and the deconvolution into two phases, hexagonal $CuInS_2$ (blue line) and hexagonal Cu_2S (pink line). (b) the crystallite shapes (arbitrarily scaled) of the two phases resulting from refinement according to the applied size-strain model. (c) reconstructed pole figures resulting from refinement according to the applied texture model. Texture was constrained to be identical for both phases.

nanoparticles, since also the hybrid materials forming in the beginning of the reaction can be converted to pure CIS nanoparticles (Figure 5b).

Furthermore, phenanthroline treatment influences the surface composition of the resulting CIS particles. The latter results in an increased aggregation tendency of the particles treated with phenanthroline, as can be seen in the TEM images (Figure 5b). Our finding can be explained taking into account the different chemical properties of copper(I) and indium(III), one being a soft and the other a hard Lewis acid. Surface copper atoms will be preferentially stabilized with thiols. The thiols set free after phenanthroline treatment, being soft Lewis bases, are not suitable to stabilize an indium rich surface. This decreases the colloidal stabilization of the sample. Restoring a good colloidal stability turned out to be possible by an additional surface treatment with a hard base, for example a carboxylic acid (oleic acid in our experiment).

3.3. Formation Mechanism of the $CuInS_2$ Nanocrystals. We have studied the formation and growth of CIS nanocrystals by taking samples at different time from the reaction vessel and analyzing them with absorption spectroscopy, TEM, XRD, and EDX. A large number of samples was evaluated for this purpose

(39) Wang, F.; Tang, R.; Kao, J. L.; Dingman, S. D.; Buhro, W. E. *J. Am. Chem. Soc.* **2009**, *131*, 4983.

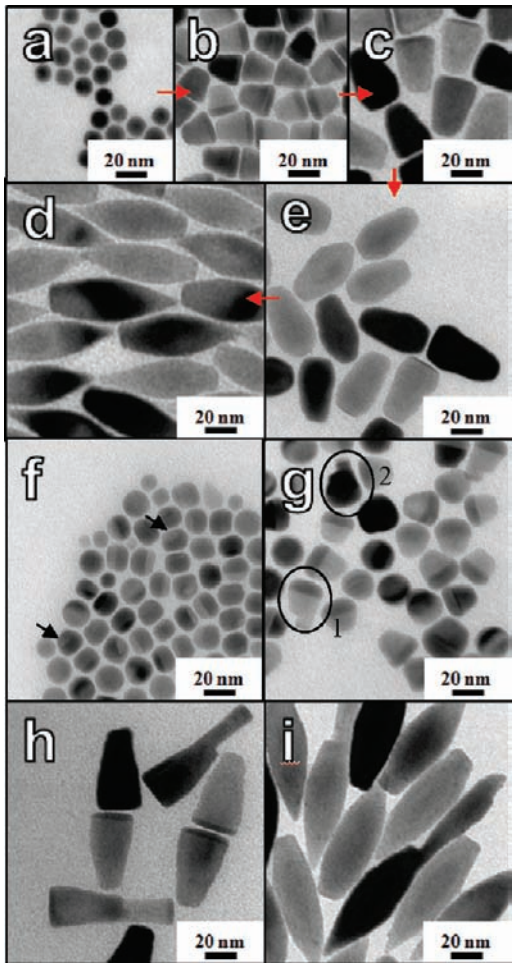

Figure 7. TEM images showing different growth stages of $CuInS_2$ nanocrystals. (a): Cu_2S particles forming in the beginning of the reaction. Images b−e show particles obtained in a reaction with Cu:In 1:1 (b): 60 s, (c): 75 s, (d): 80 s, and (e): 90 s). In (f) an early stage of the CIS nanoparticles growth is shown, the arrows depicting examples of particles, where the growth of CIS inside of Cu_2S can be seen. Different growth stages of particles obtained under conditions of faster CIS growth (compared to a−e) with a Cu:In ratio of 0.5:1 are shown in (g)−(i).

out of which only a small selection can be presented in detail here. The particles forming at the beginning of the reaction (aliquots taken 30−60 s after injection of the sulfur source) could be identified as copper sulphide. The copper−sulfur system can form a variety of different crystalline structures, and, according to the XRD measurements, a mixture of different phases seems to be present (see Supporting Information).

Hexagonal Cu_2S and CIS have the same anion lattices, which makes an epitaxial growth of one of the material onto the other possible. Also, a conversion of Cu_2S to CIS requires little lattice distortion and does not have a high energy barrier. At the reaction temperature (240 °C), the copper ions in Cu_2S have a relatively high mobility, which can facilitate an exchange with In ions and a chemical transformation to CIS.

In Figure 7, representatively selected nanoparticles obtained at different stages of the reaction are shown. In the first step, spherical copper sulphide particles are formed (Figure 7a). Then a formation of a second phase can be observed, and Cu_2S−$CuInS_2$ nanoparticles are obtained (Figure 7b). Closer inspection suggests that the formation of a CIS nucleus takes place inside the copper sulphide particles, yet not on their surface, as can be seen in some particles from the TEM

Scheme 1. Scheme of the Growth Mechanism of CIS Nanoparticles

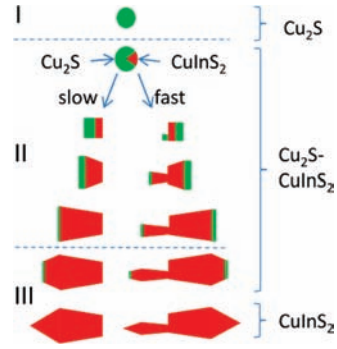

images taken at early stages of the reaction (Figure 7f,g and Figure S8 of the Supporting Information). Further growth of the CIS part of the hybrid material is accompanied by some rearrangement of the copper sulphide phase from a spherical to a disk shape (Figure 7b,c). This stage of the reaction gives us the possibility to influence the final shape of CIS nanoparticles.

The further growth of the CIS phase seems to take place only on the interface between the two materials: When choosing conditions for relatively fast growth of the CIS phase (e.g., by using some In excess), the copper sulphide part of the nanoparticles is divided into two parts, situated at two ends of the CIS phase, and further growth of the CIS phase in two directions is observed, the diameters of both parts being controlled by the size of both copper sulphide particles (Figure 7g−i, see in particular the marked particles in Figure 7g). Apparently, no perfect rearrangement of the copper sulphide part is possible under these conditions of fast growth. Most of the particles are divided into two parts of different sizes, which gives rise to the formation of dimeric CIS nanorods with two different widths and lengths (Figure 7h,i).

The results of the above reaction clearly show the role of copper sulphide in the formation and shape control of CIS nanoparticles. Both parts of the asymmetric dimers form simultaneously under otherwise identical conditions (temperature, monomer supply). The only difference between them is the size of the respective copper sulphide part of the hybrid structure (e.g., particles 1 and 2 in Figure 7g). An analysis of the TEM images demonstrates that smaller copper sulphide particles lead to the formation of CIS nanorods with smaller diameter and their conversion to CIS is faster than in the case of bigger particles, which also influences the length of the CIS nanorods generated. In slower reactions (Cu:In ratio 1:1), the copper sulphide part of the hybrid material has enough time to rearrange and to form only one disk (see Figure 7b,c). This results in the growth of extremely uniform CIS particles (Figure 7d,e).

On the basis of these observations, we propose that the reaction has three steps, illustrated in Scheme 1. At the beginning, copper sulphide nanoparticles form (phase I), in a second step, these particles serve as starting point for anisotropic growth of CIS. During this stage of the reaction, the diameter of the copper sulphide disk increases, while its thickness decreases, and CIS regions of the nanoparticles grow (phase II). Depending on the growth kinetics, the Cu_2S particles can remain one single part (slow regime) or be splitted into two parts (fast regime). The growth of CIS goes on also in the third step of the reaction (phase III, see also Figure 7d), when the

copper sulphide parts of the nanohybrids get smaller and, finally, disappear completely. Thus, as an intermediate stage, we obtain hybrid nanoparticles composed of Cu_2S and CIS, the copper sulphide part disappearing later in the course of the reaction.

Use of copper sulphide nanoparticles as a starting point for the nucleation of another material has already been reported for $Cu_2S-In_2S_3$ hybrid materials[30,31] and CIS nanorods.[32] In the case of $Cu_2S-In_2S_3$, uniform particles with different shapes as well as core−shell structures could be obtained. The report on CIS nanorods was the first one, where monophasic CIS particles were synthesized using Cu_2S seeds. Despite the similarity in the synthetic method, our approach gives an additional possibility to control the shape of the nanoparticles and yields samples with much narrower size distribution. In our reaction, the diameter of the Cu_2S particle controls the width of the emerging CIS nanocrystal. The growth of CIS stops when the complete Cu_2S part of the nanoparticle has been converted to CIS and we do not observe any significant changes in the shape of the particles after their growth has ended. Hence, controlling both nucleation and growth of the copper sulphide phase is the key to control the shape of CIS nanocrystals. In the following, some examples will be given for the possible shape control by our method. For a better comparison of the results, all TEM images in the present and next section are shown at the same magnification.

3.4. Size and Shape Control. We have studied the formation of CIS nanocrystals under various reaction conditions, systematically changing the ratio between the starting materials (CuAc, $InAc_3$, TOPO, 1-DDT, *t*-DDT) and their overall concentration. It turned out that the final shape of CIS nanoparticles mainly depends on three parameters: the amount of TOPO (regulating the activity of the In monomers), the ratio between 1-DDT and CuAc (influencing the activity of Cu monomers) and the amount of *t*-DDT (mainly responsible for the sulfur supply for the reaction). Lowering the activity of one of the components will stop the reaction at an earlier stage, which results in smaller (shorter) particles. The overall concentration of the reaction mixture turned out to influence the shape of the particles to a much smaller extent than the ratio between the educts.

Figure 8 shows different modifications of the elongated shape obtained by changing the reaction conditions. The amount of TOPO (90%) turned out to have some influence on the length of the particles. Longer particles could be obtained in reactions with a smaller amount of TOPO (Figure 8a), while shorter ones grow when the amount of TOPO has increased (Figure 8b). This can be due to the reduced activity of In in TOPO rich reactions and the depletion of monomers through the growth of nanoparticles. An influence of the amount of TOPO on the nucleation step might also be a reason for obtaining longer particles with less TOPO. However, this explanation seems less likely, because absorption spectra taken at an early stage of growth did not provide evidence for an influence of the TOPO amount on the concentration of seeds.

Another possible explanation is the enhanced surface stabilization by TOPO and the impurities present in technical grade TOPO,[38,39] which can also strongly bind to the surface of CIS nanocrystals. Comparison of this shape to the wurtzite crystal structure reveals that the tips can be terminated by cation rich (1−11) facets. The angle between the [001] direction and (1−11) facets is 27.8°, and indeed, the tips of the nanocrystals in Figure 8 b form a ∼30° angle with the *c*-axis. Addition of TOPO can increase the stabilization of the In sites of these facets and slow down further growth.

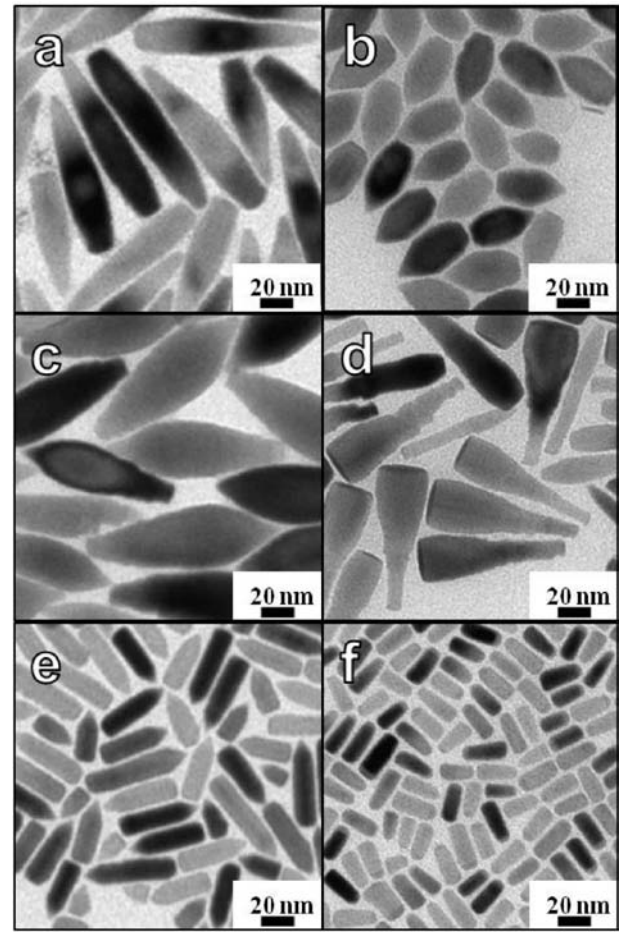

Figure 8. Different aspect ratio of CIS nanocrystals. Reaction conditions: (a) Cu:In:TOPO 1:1:4.4, 0.25 mL 1-DDT, 1.75 mL *t*-DDT; (b) Cu:In:TOPO 1:1:10, 0.25 mL 1-DDT, 1.75 mL *t*-DDT; (c) and (d) Cu:In:TOPO 1:1:3, 0.75 mL 1-DDT, 5.25 mL *t*-DDT, image (d) showing an intermediate stage of the reaction; (e) and (f) Cu:In:TOPO 1:1:3.5, 0.5 mL 1-DDT, 1.5 mL *t*-DDT, particles in image (f) were found in an aliquot taken in an early stage of the reaction conducted with double overall concentration compared to (e).

Also, the variation of the amount of both thiols turned out to have a strong influence on the shape of the elongated particles. Increasing the amount of the sulfur source leads to the formation of fish-shaped particles of up to 120 nm length and a maximum width of 40 nm (Figure 8c). When stopping the reaction at an earlier growth stage, bottle shaped Cu_2S-CIS hybrid particles can be obtained (Figure 8d). An increased amount of sulfur in the reaction mixture allows for growing larger particles. One possible reason will be simply the availability of more material for the growth of CIS. However, in all other reactions, the sulfur source is also used in a more than 10-fold excess. So a more probable reason for the influence of the sulfur amount on the growth of CIS nanoparticles will be its impact on the Cu_2S part of the hybrid nanoparticles during the growth process. The availability of more sulfur enhances the duration of the second phase of the growth (see Scheme 1) and, probably, enables growth of the Cu_2S phase of the hybrid material, in parallel to the growth of CIS, or, at least, delays it conversion to CIS. The size distribution of these samples however, is broader than in other cases, and the width of the particles much less uniform.

Samples uniform in width can be obtained by increasing the amount of 1-DDT. Two examples of particles synthesized in this way are shown in Figure 8e,f. Pencil-shaped particles in

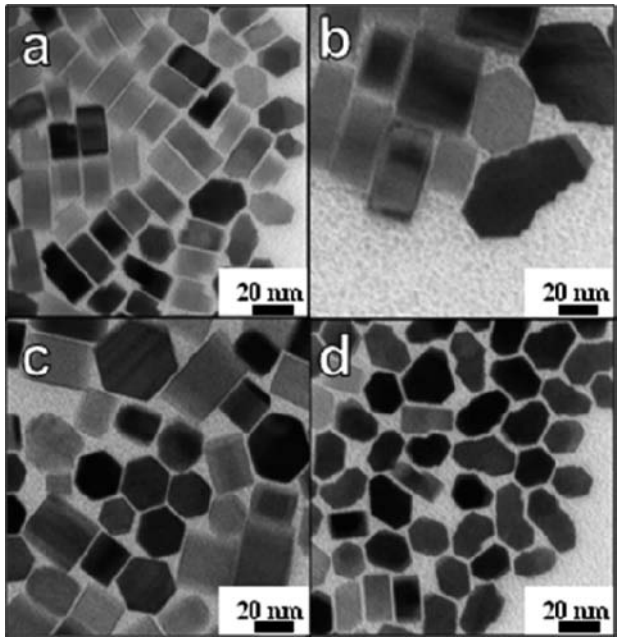

Figure 9. Hexagonal CIS platelets obtained (a) by increasing the amount of TOPO (90%): Cu:In:TOPO 1:1:50, and by addition of phosphonic acids: (b) methylphosphonic acid and (d) octylphosphonic acid. (c) Particles synthesized by using chlorides instead of acetates, under otherwise the same reaction conditions as described in the Experimental Section.

Figure 8e are pure CIS crystals, whereas Figure 8f shows an intermediate step (of another reaction) with Cu_2S still present. The shape of the tips of the pencil-shaped particles again gives rise to the assumption that they are terminated by cation rich (1−11) facets (see the discussion above to Figure 8b). Probably increased stabilization of Cu sites of these facets by the help of 1-DDT gives rise to the formation of such a shape. The higher concentration of 1-DDT decreases the activity of Cu monomers and also influences the stabilization of the Cu_2S parts of the hybrid nanostructures. So, the diameter of the Cu_2S nanodiscs does not change during growth of the CIS particles, which results in their uniform width. It should also be noted, however, that increasing the amount of 1-DDT has some influence on the nucleation step of the reaction and larger amounts of 1-DDT broaden the size and shape distribution of the particles by slowing down the nucleation process.

The samples described until now had elongated shapes with a preferential growth direction along the *c* axis. Increasing the amount of TOPO (90%) by about 10× leads to a structural change from elongated to flattened, hexagonally shaped, faceted particles. In Figure 9a, a typical overview TEM image of such a sample is shown. Obviously, two different orientations of the particles can be seen, with the *c*-axis oriented parallel or perpendicular to the TEM grid, the rectangular shapes resulting from the orientation of the *c*-axis parallel to the substrate. An analysis of about 200 rectangular particles revealed that these particles have a thickness (dimension parallel to the *c*-axis) of 20 ± 3 nm and a diameter of 26 ± 7 nm. Figure 10a gives the XRD pattern of such a sample. Rietveld analysis also confirms that these particles only contain pure $CuInS_2$. Size-shape analysis confirms a crystallite shape of platelets with the *c*-axis being the short axis (see Figure 10b). The texture analysis which has been simultaneously performed revealed that the *c*-axis is preferentially orientated perpendicular to the substrate (see

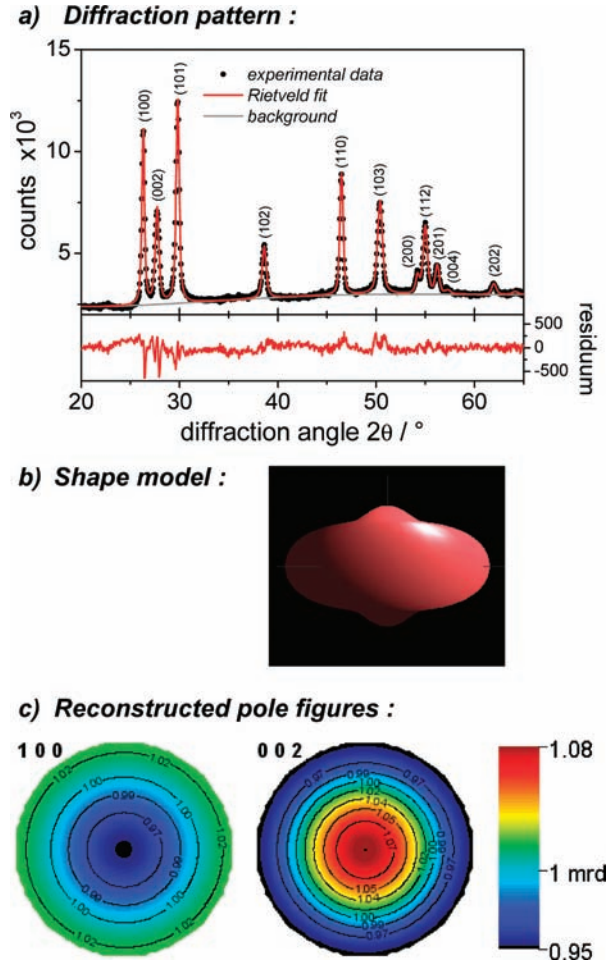

Figure 10. (a) Diffraction pattern of a typical sample similar to those in Figure 9. The experimental data (dots) is plotted together with a Rietveld fit (red line). (b) The crystallite shape resulting from refinement according to the applied size-strain model. (c) Reconstructed pole figures resulting from refinement according to the applied texture model.

Figure 10c) which appears reasonable for this shape. Table S1 in the Supporting Information reports more details on the fitting parameters.

We repeated the above reaction with higher purity TOPO (98%) and again obtained particles being elongated along the *c*-axis (shapes similar to particles shown in Figure 1). So, not TOPO, but the impurities in the technical grade TOPO must have been responsible for the shape control in the first reaction. Such findings motivated us to repeat reactions with 98% TOPO and an addition of phosphonic acids (methylphosponic acid, octylphosphonic acid, decylphosphonic acid, and tetradecylphosphonic acid), being some of the impurities that can be found in TOPO.[38,39] Indeed via adding of phosophonic acids, again hexagonal disk shaped particles could be obtained. Figure 9b,d shows two examples of shape control, obtained with methylphosphonic acid and octylphosphonic acid, respectively. Also using chlorides instead of acetates as starting material for the synthesis turned out to be a possibility to arrive at hexagonally shaped particles (Figure 9c). Chloride and phosphonic acids are strong ligands, which lower the activity of the monomers and the chemical potential of the reaction mixture. This can explain why thermodynamically more stable faceted crystals are formed under these conditions.

Interestingly, the conditions can so drastically change during one reaction that particles having started to grow along the *c*-axis

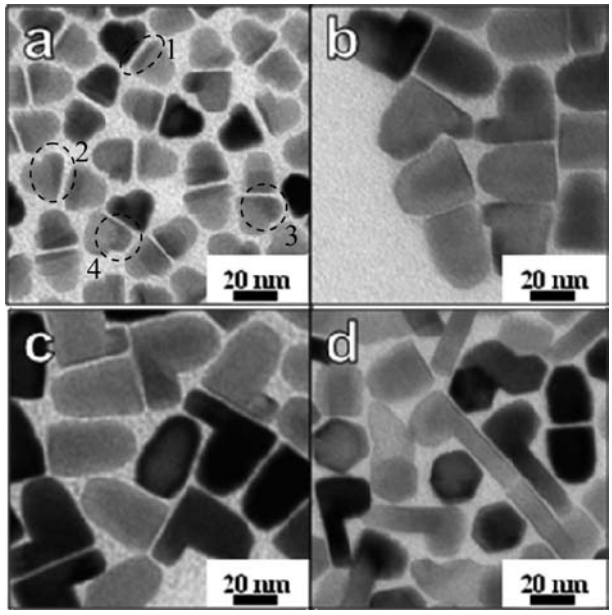

Figure 11. P-shaped nanoparticles of the Cu_2S-CIS hybrid material. (a) Cu:In:TOPO 3:1:10, 70 s growth time, (b) Cu:In:TOPO 2:1:10, 4 min growth time, (c) Cu:In:TOPO 1.5:1:10, 60 s growth time, and (d) Cu:In:TOPO 1:1:50, 60 min growth time.

change the direction of their growth and continue growing perpendicular to the *c*-axis. Some examples of such P-shaped particles and the possibilities to control their exact shape are shown in Figure 11. The experimental conditions for the growth of P-shaped particles all involve reducing the activity of In monomers, compared to that of Cu. The latter can be achieved by increasing the Cu concentration (i.e., the Cu:In ratio) (Figure 11a−c), or by moderately lowering the In activity through the addition of technical grade TOPO (Figure 11d). Under these conditions, the reaction again starts with the formation of copper sulphide and, subsequently, Cu_2S−CIS nanohybrids growing along the *c*-axis. However, the rearrangement of the Cu_2S regions to nanodiscs of uniform width (particle 1 in Figure 11a) is followed by a further shape change. One part of the discs grows, while the other becomes thinner (particle 2 and 3) and, finally, the whole Cu_2S part is located in one corner of the CIS particles (particle 4), which subsequently grows in the direction perpendicular to the *c*-axis. The growth only takes place at the interface between the two phases. A closer look at the P-shaped particles unveils that they consist of a hemisphere located on top of an elongated, hexagonal platelet. The size of the hemisphere and the platelet can be controlled by the reaction conditions, like the ratio between Cu and In. The X-ray diffraction patterns of the nanoparticles obtained in this way again correspond to CIS with a wurtzite structure, a shape analysis of these complex structures is, however, not possible by XRD.

3.5. Synthesis of CuInZnS. Our synthetic procedure turned out to be also suitable for synthesizing other compounds, like $CuInS_2$−ZnS alloys. TEM images of $(CuInS_2)$−$(ZnS)_2$ nanocrystals (composition obtained by EDX) are presented in Figure 12a,b. As shown in Figure 4, the absorption can be tuned when $ZnAc_2$ is injected during the CIS synthesis. ZnS is a wide bandgap semiconductor (3.7 eV), and it has already been shown[41] that it can form alloys with CIS, which results in a blue shift of the bandgap of the resulting material, compared to CIS. The alloy formation is possible because of a small lattice mismatch of only 2.2% between CIS and ZnS.[42] Figure 4 shows

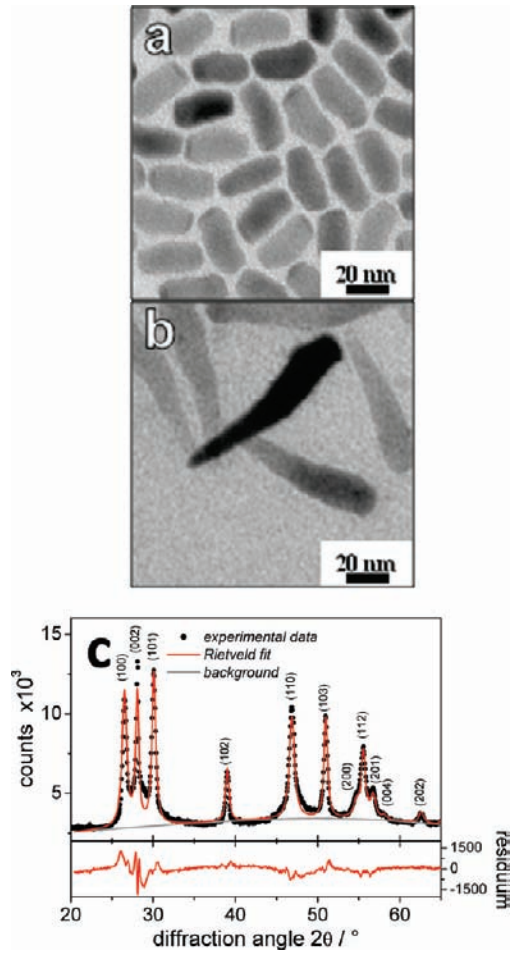

Figure 12. TEM pictures of different growth stages of alloyed CIS−ZnS nanoparticles: (a) directly after the injection of $ZnAc_2$; (b) after 1 min of growth; and (c) the XRD-pattern of the particles shown in (b).

absorption spectra of pure CIS and CIS−ZnS alloyed nanoparticles, obtained by addition of zinc acetate to the reaction mixture. Both samples contain nanorods with similar widths and length of several tens of nanometers. The absorption of the sample containing zinc is clearly blue-shifted. This effect is due to the alloy formation and, again, not a result of size quantization.

Figure 12c shows an XRD pattern of a Zn-containing sample. Basically, the same reflections as in the case of CIS are observed, but they are slightly shifted. This means that the sample has the same crystal structure, but with slightly different lattice parameters. The Rietveld fit was obtained with Cu, In, and Zn ions, randomly distributed over the Zn sites of the wurtzite ZnS structure and lattice parameters of $a = 3.874$ Å and $c = 6.349$ Å. This is a good proof for the formation of a $CuInS_2$−ZnS alloy.

4. Conclusions

A novel synthetic procedure has been described, allowing highly advanced size and shape control of CIS nanoparticles and Cu_2S−CIS hybrid nanostructures. Upon reducing the activity of the In precursor, we can avoid the homogeneous nucleation of CIS under our reaction conditions. So, in the first

(40) Will, G.; Hinze, E.; Adbelrahman, A. R. M. *Eur. J. Mineral.* **2002**, *14*, 591.
(41) Pan, D.; Weng, D.; Wang, X.; Xiao, Q.; Chen, W.; Xu, C.; Yang, Z.; Lu, Y. *Chem. Commun.* **2009**, 4221.

step of the reaction, pure Cu_2S nanoparticles grow, and CIS can only start growing inside the Cu_2S phase. Our investigations demonstrate the importance of the formation of Cu_2S nanoparticles and Cu_2S-CIS hybrid nanostructures for the shape control of CIS nanoparticles forming at the end of the reaction. Growth of CIS takes place only at the Cu_2S-CIS interface, and so the diameter of Cu_2S nanodiscs, being part of Cu_2S-CIS hybrid material controls the diameter of the growing CIS nanocrystal. As a consequence, any change of the shape of the Cu_2S nanodisc during the reaction results in a width modulation of the growing CIS nanorods. The latter can be tuned by changing the reaction conditions such that nanorods with different aspect ratio and shape come forth.

Treatment with 1,10-phenanthroline, a reagent strongly binding to copper(I) ions, turned out to be not only a possibility to remove Cu_2S parts from Cu_2S-CIS hybrid nanostructures, which results in new shapes of CIS nanoparticles, not accessible otherwise, but is also a possibility to specifically remove surface copper atoms. CIS nanocrystals with an indium rich surface can be obtained in this way.

With nanocrystals synthesized by our method being in the size range of tens of nanometers, no size quantization effects and, consequently, no tuning of the absorption properties by changing their size and shape should be expected. This motivated us to use doping with Zn as a means to change the absorption of the nanocrystals. ZnS is known to form alloys with CIS, and our method turned out to be suitable to synthesize such class of materials, too.

(42) Parasyuk, O. V.; Voronyuk, S. V.; Gulay, L. D.; Davidyuk, G. Y.; Halka, V. O *J. Alloys Compd.* **2003**, *348*, 57.

Acknowledgment. We would like to thank Erhard Rhiel (University of Oldenburg) and Heike Oetting (University of Oldenburg) for assistance in obtaining TEM images, and Dr. Marco Schowalter (University of Bremen, Germany) for taking the HRTEM images as well as the elemental analysis of single particles. We gratefully acknowledge funding by the Federal Ministry of Education and Research (BMBF, Project No. 03SF0338C) and funding of the EWE Research Group "Thin Film Photovoltaics" by the EWE AG, Oldenburg.

Supporting Information Available: Additional details on the XRD analysis of CIS nanoparticles and Cu_2S-CIS nanocomposites, XRD analysis of Cu−S nanoparticles forming at the beginning of the reaction, Study of CIS nanoparticles before and after treatment with phenanthroline (XRD, TEM), TEM image of Cu_2S-CIS nanocomposites at an early stage of the reaction. This material is available free of charge via the Internet at http://pubs.acs.org.

JA103828F